A MODIFIED NAD ALGORITHM WITH MINIMUM NUMERICAL DISPERSION FOR SIMULATION OF ANISOTROPIC WAVE PROPAGATION

DINGHUI YANG[1], GUOJIE SONG[2] and JINHUA ZHANG[3]

[1] *Department of Mathematical Sciences, Tsinghua University, Beijing 100084, P.R. China. dhyang@math.tsinghua.edu.cn*
[2] *College of Sciences, Southwest Petroleum University, Chengdu 610500, P.R. China.*
[3] *Kunming Vocational and Technical College of Industry, Yunnan, P.R. China.*

(Received March 8, 2009; revised version accepted August 8, 2009)

ABSTRACT

Yang, D., Song, G. and Zhang, J., 2010. A modified NAD algorithm with minimum numerical dispersion for simulation of anisotropic wave propagation. *Journal of Seismic Exploration*, 19: 21-42.

Conventional explicit finite-difference methods for solving the elastic-wave equation suffer from numerical dispersion when too few samples per wavelength are used. A nearly analytic discrete method for suppressing the numerical dispersion was proposed recently by Yang et al. (2003a). In this paper, we present a modified algorithm of the nearly-analytic discrete method (NADM) for modelling seismic propagation in 2D anisotropic media. We also investigate the numerical dispersion of the modified algorithm using numerical examples and compare numerically the dispersion errors and the wavefield results computed using the modified algorithm against those of our previous method and other finite-difference (FD) methods. We show that, compared with the improved NADM, the modified algorithm for the 2D case can further minimize the numerical dispersion, while its computational cost and storage space are the same as those of our previous method. Wavefield snapshot for two-layer heterogeneous medium and three-component synthetic VSP seismograms in three-layer transversely isotropic media with a vertical symmetry axis, generated using the modified algorithm, are also reported. Numerical results demonstrate that the modified algorithm further reduces the numerical dispersion and source noise caused by the discretization of elastic-wave equations when too few samples per wavelength are used or when models have large velocity contrast and strong anisotropy.

KEYWORDS: modified NAD algorithm, numerical dispersion, wavefield simulation, seismic anisotropy.

0963-0651/10/$5.00

INTRODUCTION

In anisotropic media, the seismic wave propagation becomes very complex because many wave modes such as quasi-P (qP), quasi-S (qS), converted waves, and so on simultaneously exist in anisotropic media. Therefore, modelling seismic wave propagation in complex geological media is a challenging task for most classical methods.

Given the discretized equations, the boundary conditions, and the source, we may generate the synthetic seismograms for two-dimensional geologic models of interest. However, such seismograms may contain several artifacts inherent to most classical discretization (e.g., finite-difference, finite-element) procedure, such as, grid dispersion (or called the numerical dispersion), source-generated noise (artifacts due to source location at grid points), and edge reflections. The numerical dispersion or source noise, caused by the discretization of the wave equations when too few samples per wavelength are used or when the models have large velocity contrast, or artifacts caused by source at grid points (Kelly et al., 1976; Fei and Larner, 1995; Zhang et al., 1999; Yang et al., 2002a; Zheng and Zhang, 2005), can lower the resolution of modelling results. To eliminate the numerical dispersion, one way is to use sufficient grid points per upper half-power wavelength. For example, ten or more grid points per wavelength at the frequency of the upper half-power point should be adequate when the usual second order accuracy finite-difference scheme is employed, while the fourth-order scheme seems to produce accurate results at five grid points per wavelength at the frequency of the upper half-power point (Alford et al., 1974). Dablain (1986) stated that eight and four grid points at the Nyquist frequency are required to eliminate the numerical dispersion for second-order and fourth-order finite-difference methods, respectively. However, this way using more grid points per wavelength results in needing more computational costs and storages for computer code. It is difficult to implement the large-scale application of the technique, especially for the 3-dimensional simulation of seismic wave propagation because of its intensive use of CPU time and its need for large amounts of direct-access memory. Another way of reducing the numerical dispersion is to use higher-order FD schemes (e.g., tenth-order method; Dablain, 1986) or the pseudo-spectral method (Kosloff and Baysal, 1982; Kosloff et al., 1984; Huang, 1992) or optimizing finite-difference operator method (the higher-order finite-difference algorithm) according to a required accuracy (Holberg, 1987) to reduce the numerical dispersion. The higher-order FD method requires more floating point operations, however, because, in general, it involves more grid points in a direction. The requirement of more grids in the higher-order finite-difference methods is not advantageous to implement artificial boundary treatment and efficient parallel calculations. The pseudo-spectral (PS) method is attractive as the space operators are exact up to the Nyquist frequency. In

other words, the PS method only requires two grid points per wavelength for eliminating the spatial numerical dispersion (Dablain, 1986). However, it also suffers from numerical dispersion in time, and its numerical dispersion increases with increasing the Courant number defined by $\alpha = c\Delta t/\Delta x$ (Dablain, 1986; Sei and Symes, 1994), i.e., as the time increment increases (Yang et al. 2006). For example, the PS method based on the Fourier transform means that each point interacts with every other point. To some extent, this is unphysical as the interaction in dynamic elasticity is of a local nature. Besides, we can also use the flux-corrected transport technique, which is unable to recover the lost resolution due to the numerical dispersion when the spatial sampling becomes too coarse (Yang et al., 2002a; Zheng et al., 2006).

The staggered-grid FD methods with local operators (Virieux, 1986; Fornberg, 1990; Igel et al., 1995) can further reduce the numerical dispersion, but they still suffer from the numerical dispersion when too few samples per wavelength are used (Sei and Symes, 1994; Yang et al., 2002b). Meanwhile, Igel et al. (1995) conclude that for the anisotropic case the staggered-grid FD method may result in the numerical anisotropy and induce additional error of the wave properties, due to some of the elements of the stress and strain tensors must be interpolated to calculate the Hook sum for the strain-stress staggered-grid FD.

The "nearly analytic discrete method", suggested by Yang et al. (2003a) for acoustic and elastic equations, is another effective method for decreasing the numerical dispersion. The method, based on the truncated Taylor expansion and the local interpolation compensation for the truncated Taylor series, uses the wave displacement-, the velocity and their gradient fields to restructure the wave displacement-fields. Hence it enables effectively to suppress the numerical dispersion caused by discretizing the wave equation. Recently, we improved the NADM including increasing the time accuracy and reducing the storage (Yang et al., 2007a) as the optimal NADM presented in Yang et al. (2006), but the optimal method cannot be applied to the Biot equations including the velocity $\partial U/\partial t$ of the wave displacement U because the optimal method does not compute the velocity-fields. Both the NADM (Yang et al., 2003a) and the improved NADM (Yang et al., 2007a), which involves to compute the velocity $\partial U/\partial t$, is called simply the NAD method in this article.

This paper is to present a modified algorithm of the NAD-type methods, called the modified NAD algorithm (NADA), and discuss the efficient implementation of the modified NADA. We also investigate the dispersion errors and the sampling rate per wavelength to eliminate the numerical dispersion for the modified algorithm, and compare some wave fields computed by the modified algorithm against the method of Yang et al. (2007a) and the fourth-order Lax-Wendroff correction (Dablain, 1986). Wavefield modelling shows that the modified NADA can further reduce the numerical dispersion over

the original one, while it keeps the same computational costs and storages as those of Yang et al. (2007a). Meanwhile, we also show the VSP synthetic seismograms generated by the modified NADA for the 2D transversely isotropic medium.

ANISOTROPIC WAVE EQUATION AND BASIC NAD-TYPE METHODS

Anisotropic wave equation

In 3D anisotropic media, the system of elastic wave equations can be written as

$$(\partial\sigma_{ij}/\partial x_j) + f_i = \rho(\partial^2 u_i/\partial t^2) \quad , \quad i = 1,2,3, \tag{1a}$$

$$\sigma_{ij} = \tfrac{1}{2}c_{ijkl}(x,y,z)[(\partial u_k/\partial x_l) + (\partial u_l/\partial x_k)] \quad , \tag{1b}$$

where i,j,k, $l = 1,2,3$, $\rho = \rho(x_1,x_2,x_3)$ is the density, u_i and f_i denote the displacement component and the force-source component in the i-th direction. The fourth-order stiffness tensor $c_{ijkl}(x_1,x_2,x_3)$ may have up to 21 independent elastic constants for the 3D case and satisfies the following symmetry conditions:

$$c_{ijkl}(x_1,x_2,x_3) = c_{jikl}(x_1,x_2,x_3) = c_{ijlk}(x_1,x_2,x_3) = c_{klij}(x_1,x_2,x_3) \quad .$$

Basic NAD methods

For convenience, in the following we replace the coordinate variables x_1 and x_3 in eqs. (2a) and (2b) by x and z, respectively, and take the 2D case as an example to illustrate the implementation of the NADM. The same notations as that in the basic NADM (Yang et al., 2003a) are used in our present study, i.e.,

$$U = (u_1,u_2,u_3)^T \quad , \quad \partial^2 U/\partial t^2 \equiv P,$$

$$\bar{U} = [U,(\partial U/\partial x),(\partial U/\partial z)]^T \quad ,$$

$$\bar{P} = [P,(\partial P/\partial x),(\partial P/\partial z)]^T \quad ,$$

and

$$\bar{W} = (\partial/\partial t)\bar{U} \quad .$$

Note that $\bar{W}$ is the time derivative of both the displacement component U and its first-order spatial derivatives, which is called the particle-velocity $\bar{W}$. Using the above notation with values at the time t_n and the truncated Taylor series expansion, Yang et al. (2003a) obtained the following equations

$$\bar{W}^{n+1}_{i,j} = \bar{W}^{n}_{i,j} + \Delta t\bar{P}^{n}_{i,j} + [(\Delta t)^2/2](\partial\bar{P}/\partial t)^{n}_{i,j} + [(\Delta t)^3/6](\partial^2\bar{P}/\partial t^2)^{n}_{i,j} \quad , \quad (2a)$$

$$\bar{U}^{n+1}_{i,j} = \bar{U}^{n}_{i,j} + \Delta t\bar{W}^{n}_{i,j} + [(\Delta t)^2/2]\bar{P}^{n}_{i,j} + [(\Delta t)^3/6](\partial^2\bar{P}/\partial t^2)^{n}_{i,j} + [(\Delta t)^4/24](\partial^2\bar{P}/\partial t^2)^{n}_{i,j} \quad , \quad (2b)$$

where Δt denotes the time increment.

Using original eq. (1), we convert the higher-order time derivatives of the displacement U on the right side of eqs. (2a) and (2b) into spatial derivatives, which is similar to the higher-order FD methods (Dablain, 1986; Wang et al., 2002) or the Lax-Wendroff correction schemes (Blanch and Robertsson, 1997). These higher-order spatial derivatives at grid points are determined by the displacement U and its gradients using the interpolation approximation [see Appendix B in the cited reference (Yang et al., 2003a)], while in the NADM the higher-order spatial derivatives of the particle-velocity $\bar{W}$ on the right side. are determined by a backward difference, resulting in the second-order time accuracy of the NADM.

In our recent work, we introduce similar interpolation function and connection relations to determine $\partial_{kxmz}W^{n}_{i,j}$ $(2 \le k+m \le 3)$ [see Appendix A in the cited reference (Yang et al., 2007a)], as shown in our earlier work (Yang et al., 2003a). As a result, the improved NADM, compared with the NADM, saves the storage about 37% and improves the time accuracy from second-order of the original NADM to fourth-order (Yang et al., 2007a), while the space accuracy remains the same as that of the original NADM. And like the NADM the improved NADM enjoys the same less numerical dispersion (Yang et al., 2007a). Note that the improved NADM suggested by Yang et al. (2007a) has also similar computational equation as (2).

MODIFIED ALGORITHM OF NAD-TYPE METHODS

Now let us take a closer look at eq. (2) in the NAD-type methods. To compute $\bar{U}^{n+1}_{i,j}$ at the grid-point (i,j) using eq. (2b), we need to calculate the particle-velocity $\bar{W}^{n+1}_{i,j}$ using eq. (2a) because of the involvement of the particle-velocity $\bar{W}^{n}_{i,j}$ in eq. (2b). From the computational process of the NAD-type methods using eqs. (2a) and (2b) we find that the particle-velocity $\bar{W}^{n+1}_{i,j}$ at the (n+1)-th time-level has been calculated using eq. (2a) as we use eq. (2b) to compute $\bar{U}^{n+1}_{i,j}$. Therefore, we can replace $\bar{W}^{n}_{i,j}$ in eq. (2b) by $\bar{W}^{n+1}_{i,j}$, resulting in the following alternative algorithm:

$$\bar{W}^{n+1}_{i,j} = \bar{W}^{n}_{i,j} + \Delta t\bar{P}^{n}_{i,j} + [(\Delta t)^2/2](\partial\bar{P}/\partial t)^{n}_{i,j} + [(\Delta t)^3/6](\partial^2\bar{P}/\partial t^2)^{n}_{i,j} \quad , \quad (3a)$$

$$\bar{U}^{n+1}_{i,j} = \bar{U}^{n}_{i,j} + \Delta t\bar{W}^{n+1}_{i,j} + [(\Delta t)^2/2]\bar{P}^{n}_{i,j} + [(\Delta t)^3/6](\partial^2\bar{P}/\partial t^2)^{n}_{i,j} + [(\Delta t)^4/24](\partial^2\bar{P}/\partial t^2)^{n}_{i,j} \quad . \quad (3b)$$

Note that we use the same approximations as those of the NAD methods to compute $\bar{P}^n_{i,j}$,$(\partial\bar{P}/\partial t)^n_{i,j}$, and $(\partial^2\bar{P}/\partial t^2)^n_{i,j}$ as we use the algorithm (3) to simulate anisotropic wave propagation in our present work. In other words, the higher-order spatial derivatives at the grid points, involved on the right side of eqs. (3a) and (3b), are determined by the displacement U and its gradients using the interpolation approximation as shown in the cited reference (Appendix B, Yang et al., 2003a), whereas the higher-order spatial derivatives of the particle-velocity $\bar{W}$ on the right side are determined using eqs. (A-1) to (A-7) found in our recent work (Yang et al., 2007a). For convenience, we summarize the basic idea of approximating higher-order spatial derivatives using the displacement or the particle-velocity and their gradients, and list some approximate equations in Appendix A.

Comparing algorithm (2) with algorithm (3), we can find that the only difference between algorithm (2) and algorithm (3) is to use the particle-velocity $\bar{W}^n_{i,j}$ at n-th time-level in the original NAD-type algorithm (2) and to use the up-to-date $\bar{W}^{n+1}_{i,j}$ at (n+1)-th time-level in the present algorithm (3). On the basis of such a structure, the modified NADA needs the same computational costs and storage space as the method proposed by Yang et al. (2007a), and the modified NADA also improves over the original NADM in the computational accuracy in time and increases slightly the computational costs because it employs eqs. (A-1) to (A-7) presented in Yang et al. (2007a) to determine particle-velocity $\bar{W}^n_{i,j}$. And, compared with the NADM, it saves about 37% of storage from our recent conclusions in Yang et al. (20007a).

As we have stated earlier, our present algorithm also employs the truncated Taylor series function of spatial increments and the connection relation to determine the higher-order spatial derivatives at the grid-point (i,j), the same technique as we used in the NAD-type methods. Therefore, the present algorithm enjoys several desirable properties as the NAD-type methods. It can suppress effectively the loss of wavefield information included in the higher-order terms of the infinite Taylor expansion, leading to less numerical dispersions as verified by our numerical examples. On the other hand, replacing algorithm (2) with algorithm (3), without adding any complex items such as computational costs and storage, leads to two advantages: (1) further suppressing the numerical dispersion; (2) increasing the computational convergence because we use the up-to-date $\bar{W}^{n+1}_{i,j}$ instead of $\bar{W}^n_{i,j}$. It will be verified in our latter examples. Meanwhile, using the local connection relations (A-2) greatly improves the continuity and derivability of the approximate function U^n (because U^n is an approximate variable during data processing) and its approximate gradient, resulting in further improving the continuity of stress at the points in the neighborhood of interface because of the stress expressed by the gradients of displacement components.

STABILITY CRITERIA

To keep numerical calculation stable, the temporal increment Δt must satisfy the stability condition of the modified NADA. For the 2D homogeneous case, following the Fourier analysis method we firstly obtain the growth matrix H for the modified method, in which the detail expression of the matrix H is omitted because of its complex elements, and then assume that λ_1, λ_2 and λ_p are the eigenvalues of H. We know that the scheme with the growth matrix H is stable if $|\lambda_j| \leq 1$, $j = 1,2,\ldots,p$ are satisfied. So we can obtain the stability criterion of the modified method for the homogeneous case under the condition of $\Delta x = \Delta z = h$, deriving from the conditions of $|\lambda_j| \leq 1$, $j = 1,2,\ldots,p$, as follows

$$\Delta t \leq 0.24h/c_0 \quad , \tag{4}$$

where c_0 is the wave velocity.

The stability condition for a heterogeneous medium cannot be directly determined but may be approximated using a local homogeneous method. We expect that eq. (4) is approximately correct for a heterogeneous medium if the maximal value of the wave velocity c_0 is used.

Wave velocities vary with propagation directions in anisotropic media, so the stability condition $\Delta t \leq 0.24\Delta x/v_{max}$ is used, where Δx corresponds to the spatial increment and v_{max} is the maximum qP velocity in present computations. Of course, $0.24\Delta x/v_{max}$, which corresponds to the Courant number $\alpha = v_{max}\Delta t/\Delta x = 0.24$, is not the upper limit of the interval for time increment Δt, for which the modified nearly-analytic discrete algorithm is stable, and the further theoretical stability condition will be given in a separate study.

NUMERICAL DISPERSION AND EFFICIENCY

Numerical dispersion or grid dispersion is the most significant numerical problem limiting the usefulness of point-wise discretization schemes for acoustic and elastic wave equations. This numerical artifact causes the phase speed to become a function of spatial and time increments. The relative computational merit of most discretization schemes hinges on their ability to minimize this effect. In this section, we take the transversely isotropic wave equation as an example to investigate the effect of sampling rate at a wavelength for algorithm (3) through wavefield modelling and compare the dispersion errors of different methods. In this work, the computations of generating wavefield snapshots or synthetic seismic records are performed on a Pentium 4 with 512 MB memory.

In the following numerical example, we choose the transversely isotropic medium with a vertical symmetry, which is described by five elastic constants (GPa): $c_{11} = 30$, $c_{13} = 8.4$, $c_{33} = 25$, $c_{44} = 10$, $c_{66} = 8$, and the density $\rho = 2.1$ g/cm^3. The size of the computational domain is 5.54 km $\times$ 5.54 km for the acoustic case (case 1) and 10.24 km $\times$ 10.24 km for the elastic case (case 2), respectively, and all their boundaries are free surfaces. An explosive force is applied exactly at the centre of the domain. The source time function is a Ricker wavelet with a dominant frequency $f_0 = 20$ Hz. The different spatial sampling rates is chosen so that we test the effects of sampling rate based on the Nyquist frequency, which is defined by Dablain (1986)

$$\Delta x = v_{min}/(f_N \cdot G) \quad , \tag{5}$$

where v_{min} denotes the minimum qS-wave velocity, f_N is the Nyquist frequency, and G denotes the number of grid points per minimum qS wavelength along the slowest axis of the medium at the upper half-power frequency of the source (Alford et al, 1974) or the number of grid points needed to cover the Nyquist frequency for nondispersive propagation (Dablain, 1986). In this case chosen that implies a Nyquist frequency of 40 Hz.

Example 1

In the acoustic wave modelling, the spatial and time increments are chosen as $\Delta x = \Delta z = 27.7$ m and $\Delta t = 0.0015$ sec, resulting that the number of grid points per minimum wavelength is two as the minimum wave velocity is about 2.2174 km/s for the acoustic wave, and the approximate stability condition given previously is kept. Snapshots of acoustic propagation at time 0.6 s are shown in Fig. 1, generated respectively using the fourth-order Lax-Wendroff correction (LWC) (Dablain, 1986), the method of Yang et al. (2007a), and the modified NADA. We can see that the wavefronts of seismic waves shown in Fig. 1 are identical. However, the wavefield snapshot (Fig. 1c), generated using the modified NADA, shows that the modified NADA has almost no numerical dispersion and source noise even if the space increment chosen is 27.7 m (G=2) without any additional treatments, whereas the fourth-order LWC scheme suffers from serious numerical dispersions (see Fig. 1a) and the improved NADM (INADM) (Yang et al., 2007a) causes slightly numerical dispersion (Fig. 1b). Fig. 2 shows the primary arrivals at receivers R1 (3.435 km, 2.216 km) and R2 (3.324 km, 2.77 km), computed using the fourth-order LWC scheme, the improved NADM, and the modified NADA, respectively. In Figs. 2a and 2b generated using the fourth-order LWC scheme and the INADM we can see the anomalous dispersion behind the exact signal, whereas the waveform (Fig. 2c) computed using the modified NADA shows no anomalous dispersion. It further demonstrates that the modified NADA can effectively suppress the numerical dispersion and source noise.

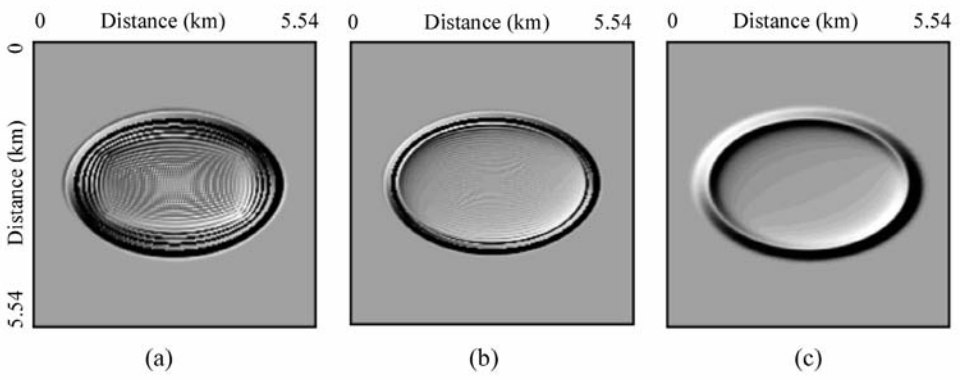

Fig. 1. Snapshots of seismic wavefields at time 0.6 s on the coarse grid ($\Delta x = \Delta z = 27.7$ m) that corresponds to G = 2, generated by the fourth-order LWC method (a), the INADM (b), and the modified NADA (c).

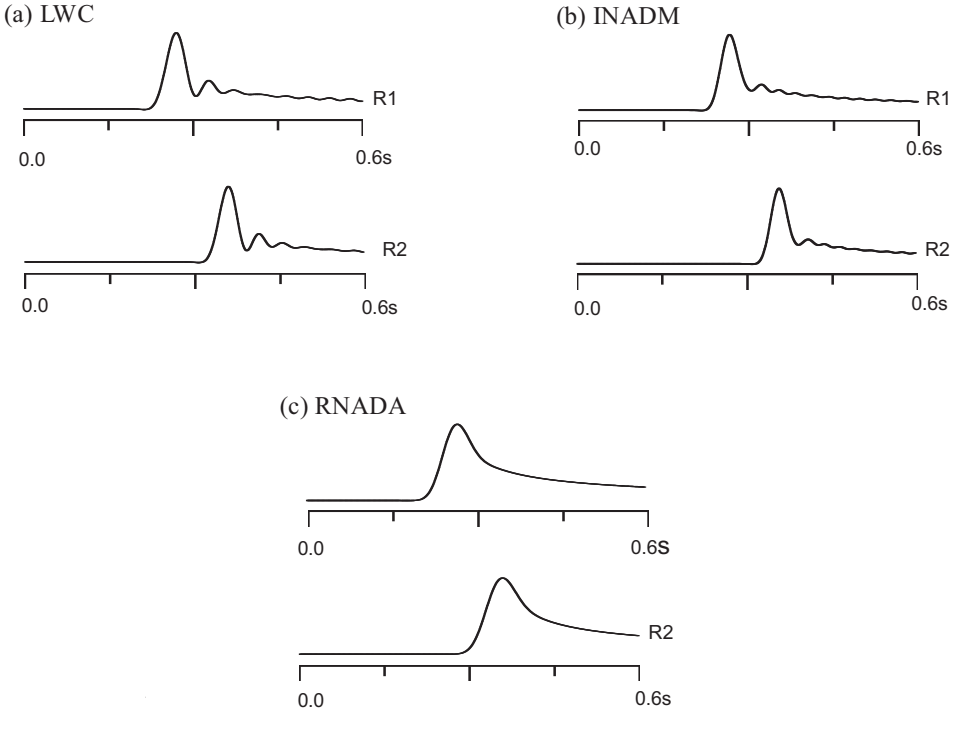

Fig. 2. A comparison of the acoustic waveforms for case 1. The synthetic seismograms (a), (b) and (c) are generated by fourth-order LWC method (Dablain, 1986), the INADM, and the modified NADA, respectively.

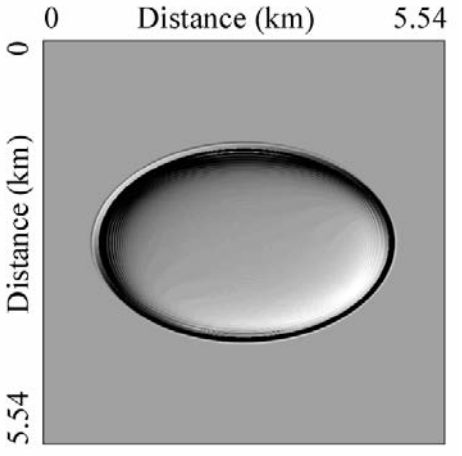

Fig. 3. Snapshot of seismic wavefields at time 0.6 s on the fine grid ($\Delta x = \Delta z = 9.2$ m) that corresponds to G = 6, generated by the fourth-order LWC method (Dablain, 1986) for case 1.

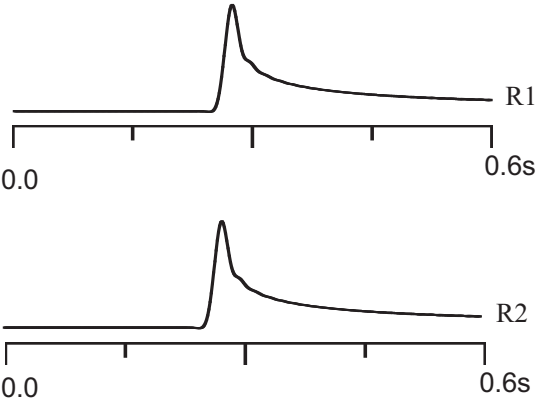

Fig. 4. Waveforms on the fine grid ($\Delta x = \Delta z = 9.2$ m) that corresponds to G = 6, generated by the fourth-order LWC method (Dablain, 1986) for case 1.

To compare the computational costs between the modified NADA and the LWC method, we also present the snapshot Fig. 3 and the waveform Fig. 4 on the fine grid $\Delta x = \Delta z = 9.2$ m (G=6) and $\Delta t = 4.982 \times 10^{-4}$ s, generated using the fourth-order LWC method. Comparison between Fig. 1c and Fig. 3 or Fig. 2c and Fig. 4 demonstrates that the modified NADA can provide the

same accuracy as that of the LWC with fourth-order accuracy on a fine grid under the same Courant number defined by $\alpha = c_0\Delta t/\Delta x$ (Dablain, 1986; Sei and Symes, 1994) with the wave velocity c_0. But the computational cost of the modified NADA is quite different from that of the LWC method. For example, it took the modified algorithm about 33 s to generate Figs. 1c or 2c, whereas the LWC method took about 435 s to generate Figs. 3 or 4. This suggests that the computational speed of the modified NADA is roughly 13 times of the fourth-order LWC on a fine grid to achieve the same accuracy as that of the modified algorithm. Note that the computational cost of the modified algorithm is more expensive than the higher-order LWC on the same coarse grid. Meanwhile, the storage space required for computation in the modified algorithm is also different from that of the LWC method. Through similar analysis in our previous work (Yang et al., 2006), we know that for the acoustic case the number of total arrays involved in the modified NADA is 12 for a typical implementation, and the number of grid points is 201 $\times$ 201 on a coarse grid for generating Figs. 1c or 2c. The fourth-order LWC method needs only three arrays to store the wave displacement at each grid point, but the number of grid points on a fine grid for generating Fig. 3 or 4 goes up to 600 $\times$ 600 for eliminating the numerical dispersion. It indicates that the modified NADA requires only roughly 45% of storage space of the fourth-order LWC while the modified algorithm needs the same storage space and computational costs as the INADM, as stated earlier.

Example 2

In the elastic wave modelling, the spatial and time increments are chosen as $\Delta x = \Delta z = 25.6$ m and $\Delta t = 0.001$ sec, corresponding to $G = 2$ because of the minimum qSV wave velocity of 2.0495 km/s for the qSV wave. Figs. 5 and 6 are the horizontal and vertical component snapshots at time 1.0 s generated using the modified NADA and the fourth-order LWC, respectively. In Fig. 5 and 6, we can see that the wavefronts of seismic waves simulated using two kinds of methods at the same time are basically identical. However, the snapshots in Fig. 6 simulated using the fourth-order LWC present strong numerical dispersion, and the corresponding results in Fig. 5 computed using the modified algorithm show that the modified NADA has almost no numerical dispersion even if the sampling rate per minimal wavelength is $G = 2$ without any additional treatments. In other words, when G goes up to the minimum grid points (two points) (Dablain, 1986) per wavelength for eliminating the spatial numerical dispersion, our present algorithm can also produce the acceptable clear wave fields. It implies that we can minimize the computational costs and storage through choosing the significant maximum spatial increment defined by $\Delta x_{max} = v_{min}/2f_N$. The wavefield simulation (Fig. 5) exhibits strong anisotropy, with typical curved qP and qSV modes, and clear cusps of qSV mode. All modelling results do not exhibit significant noise and numerical dispersion.

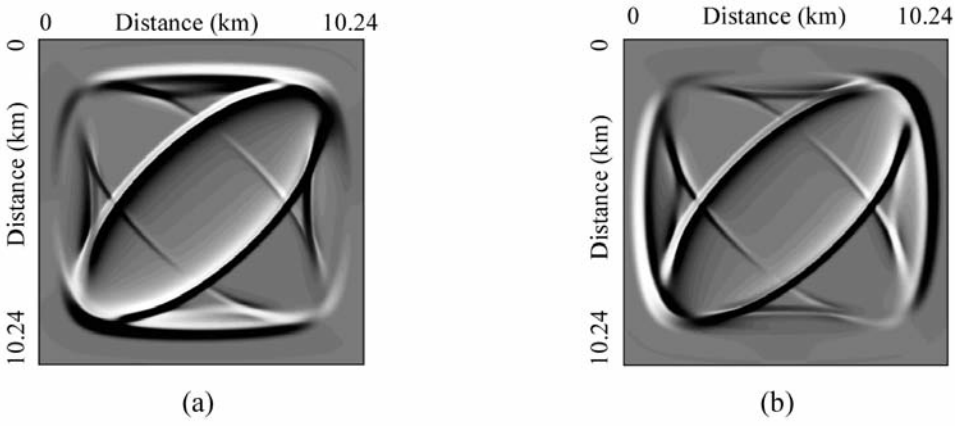

Fig. 5. Snapshots of seismic wavefields for horizontal- and vertical-components at time 1.0 s in the anisotropic medium (case 2), generated by the modified NADA, for (a) u_x component, (b) u_z component.

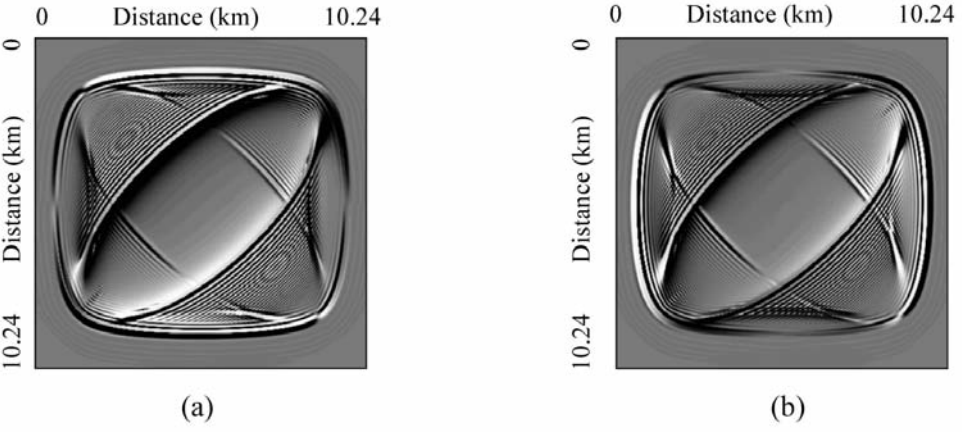

Fig. 6. Snapshots of seismic wavefields for horizontal- and vertical-components at time 1.0 s in the anisotropic medium (case 2), generated by the fourth-order LWC method, for (a) u_x component, (b) u_z component.

For further comparison, we also present the waveforms (Figs. 7a and 7b) of the horizontal component, which are the primary arrivals at receiver R1 (4.608 km, 6.144 km), generated using the modified NADA and the fourth-order LWC, respectively. From Fig. 7b computed using the fourth-order LWC, we can see the anomalous wave between the qP- and qSV-wave signals, whereas the waveform (Fig. 7a) computed using the modified NADA shows no

anomalous wave. It further verifies that our present algorithm, using the up-to-date value $\bar{W}_{i,j}^{n+1}$ in eq. (3b), can indeed minimize the numerical dispersion even for the minimum number of grid points (two points) per minimum qSV wavelength.

To deeply investigate the improvement of the numerical dispersion of the modified nearly-analytic discrete algorithm, following the analysis methods of the cited references (Vichnevetsky, 1979; Dablain, 1986; Wang et al., 2002; Yang et al., 2006) we give numerically the dispersion relation of the modified nearly-analytic discrete algorithm for the 1D case, depending on the Courant number of the method. And compare these dispersion errors of the fourth-order Lax-Wendroff correction, improved nearly-analytic discrete method, and the modified nearly-analytic discrete algorithm.

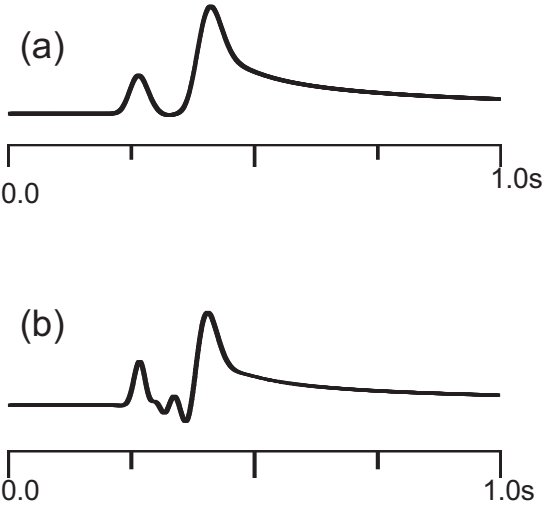

Fig. 7. Waveforms of the horizontal component on the coarse grid ($\Delta x = \Delta z = 25.6$ m) that corresponds to $G = 2$ for case 2, generated by the modified NADA for (a) and the fourth-order LWC method for (b), respectively.

Fig. 8 shows the dispersion relations for the fourth-order Lax-Wendroff correction, improved nearly-analytic discrete method, and the modified nearly-analytic discrete algorithm for the 1D homogeneous wave equation corresponding to different Courant numbers, which are shown in Figs. 8(a), (b), and (c), respectively. From Fig. 8 we can observe that the dispersion error of the modified NADA is the smallest among these errors of three algorithms in the chosen Courant ranges. From a mathematical point of view, because the modified nearly-analytic discrete algorithm uses the up-to-date $\bar{W}_{i,j}^{n+1}$ to replace the old value $\bar{W}_{i,j}^{n}$ in algorithm (3b), it increases the computational convergence, resulting in the further reduction of dispersion error of the modified

nearly-analytic discrete algorithm. This is the reason why Fig. 1(c) and Fig. 5 are clearer than Figs. 1(a), 1(b) and Fig. 6, respectively. Fig. 8(a) also shows that the numerical velocity of the modified nearly-analytic discrete algorithm gradually approximates the exact wave velocity while the Courant number α increases in the high frequency range, whereas the dispersion errors of the fourth-order LWC and the modified NADM are not sensitive to the Courant number α. This suggests that we can further minimize the dispersion error caused by the modified nearly-analytic discrete algorithm using a suitable Courant number. For example, when we choose the Courant number in $0.15 \sim 0.2$, the modified nearly-analytic discrete algorithm will have no visible numerical dispersion and source noise.

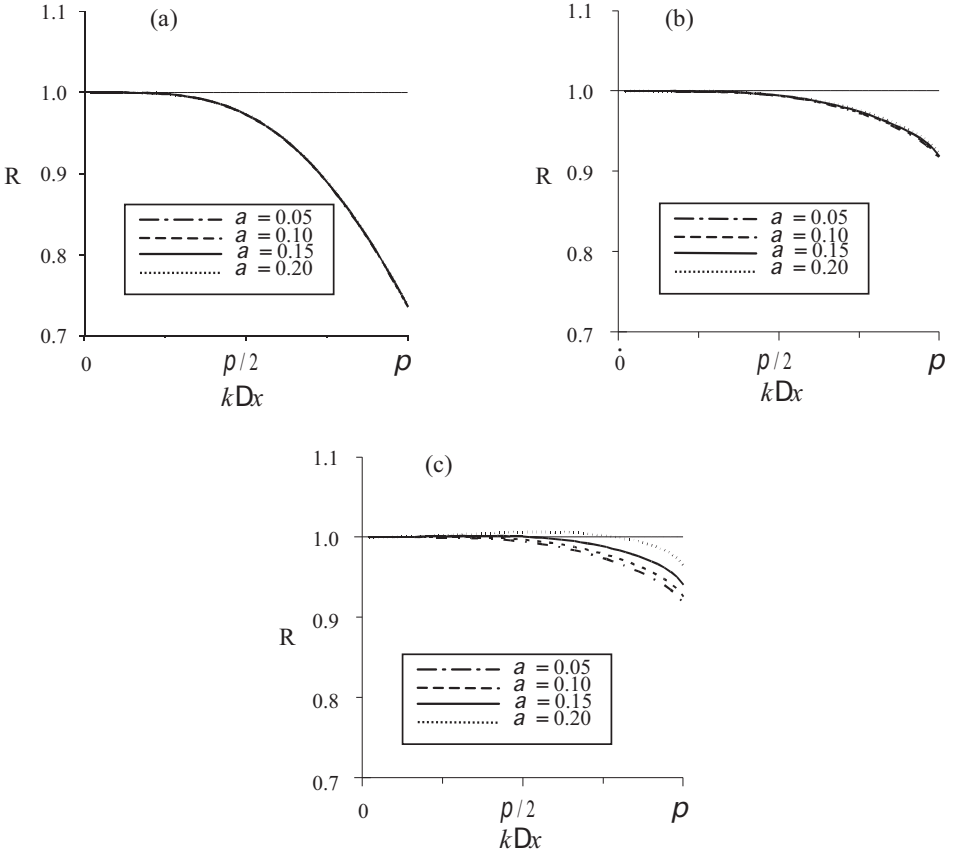

Fig. 8. The ratio of the numerical velocity to the phase velocity versus wavenumber $k\Delta x$ for the three different methods of the fourth-order LWC method, INADM, and the modified NADA for different Courant numbers $\alpha = c_0\Delta t/\Delta x$, where four lines correspond to $\alpha = 0.05$, 0.1, 0.15 and 0.2, respectively.

SYNTHETIC MODELLING

To further validate the algorithm (3), and to show that we can handle heterogeneous media, in this section we consider the transversely isotropic models of two-layer heterogeneous medium (model 1) and three-layer medium (model 2), and present the wavefield modelling results computed using the algorithm (3).

Heterogeneous, anisotropic model

In this example, we choose the two-layer medium model composed of two half-spaces: a transversely isotropic medium on the left and an isotropic material on the right. Similar model has been used to test the spectral element method (Komatitsch et al., 2000). The mechanical properties of the anisotropic and isotropic media are listed in Table 1. The computational domain is 5.744 km $\times$ 5.744 km. The spatial and time increments are chosen respectively as $\Delta x = \Delta z = 14.36$ m and $\Delta t = 3.59 \times 10^{-4}$ s, and the number of grid points 401 $\times$ 401. The source is an explosive source located 301 m to the left of the interface in the anisotropic half-space. The source time function is a Ricker wavelet with the dominant frequency $f_0 = 20$ Hz, resulting in 2.5 grid points per minimum qS wavelength along the slowest axis of the medium because of the minimal qS-velocity of 1437 m/s.

Table 1. Mechanical properties of the two-layer elastic medium used in the heterogeneous model, which is composed two half-spaces: a transversely isotropic medium on the left and an isotropic material on the right.

Layer	Thickness	c_{11}	c_{13}	c_{33}	c_{55}	ρ
	(km)	(GPa)	(GPa)	(GPa)	(GPa)	(g/cm^3)
Anisotropic	2.872	16.5	5	6.2	3.96	1.78
Isotropic	2.872	16.5	8.58	16.5	3.96	1.78

Fig. 9 shows the wavefield snapshot of horizontal component of displacement at time 0.8 sec, generated using the algorithm (3). Fig. 9 shows numerous phases such as direct qP-wave, direct qS-wave, and their reflected, transmitted, converted phases, and so on, which are labeled in Fig. 9. We can clearly see from Fig. 9 that the wavefront of qS-wave is an ellipse in the left layer and is a cycle in the right layer, and the qS wavefronts can have cusps and

triplications depending on the value of c_{13} (Faria and Stoffa, 1994). Triplications can be observed in the horizontal component qS-wavefronts shown on the left layer in Fig. 9, which also shows that the modified NADA has less numerical dispersions without any additional treatments even if the number of grid points per minimum wavelength is about 2.5 and the model velocity contrasts between adjacent layers are 1.63 times. On a Pentium 4 with 512 MB memory, it took roughly 9 min to generate the results shown in Fig. 9.

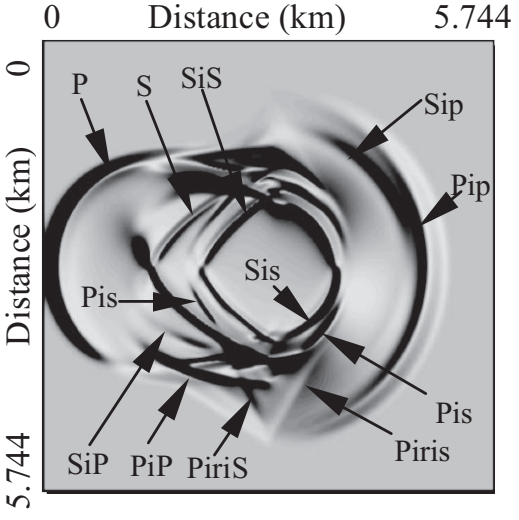

Fig. 9. Wavefield snapshot of the horizontal u_x component at time 0.8 s for a heterogeneous medium, generated by the modified NADA.

Three-layer anisotropic model

In the final example, we choose the three-layer anisotropic model that mechanical properties of the model are summarized in Table 2. The geometry is illustrated in Fig. 10. The source is an explosive source located at the depth of z = 0.3 km and the distance between the source to the first receiver is 8.55 km. The source time function is a Ricker wavelet with the dominant frequency f_0 = 20 Hz. The degrees of qS-wave anisotropy are about 11.8%, 17.3%, and 11.8%, corresponding to layers 1, 2 and 3, respectively. The computational domain is 10 km × 10 km. A grid size of 50 m in x- and z-direction is chosen. The time sample rate is 0.0025 s. The wavefields are recorded in well by 201 receivers for the tree-layer anisotropic model spread from the surface (z = 0) to the depth of 10 km spaced 50 m apart. Absorbing boundary conditions suggested by Yang et al. (2003b) are used on the three edges (left and right boundaries, and bottom boundary) of the grids and the free boundary condition (stiff boundary condition) is used on the surface.

Table 2. Mechanical properties of the three-layer anisotropic medium used in model 2, which is the same elastic property of layer 1 as that of layer 3.

Layer (No.)	Thickness (km)	c_{11} (GPa)	c_{13} (GPa)	c_{33} (GPa)	c_{44} (GPa)	c_{66} (GPa)	ρ (g/cm^3)
1	5	30	8.4	25	10	8	2.1
2	2.5	20	6.4	19	5.5	4	3.5
3	2.5	30	8.4	25	10	8	2.1

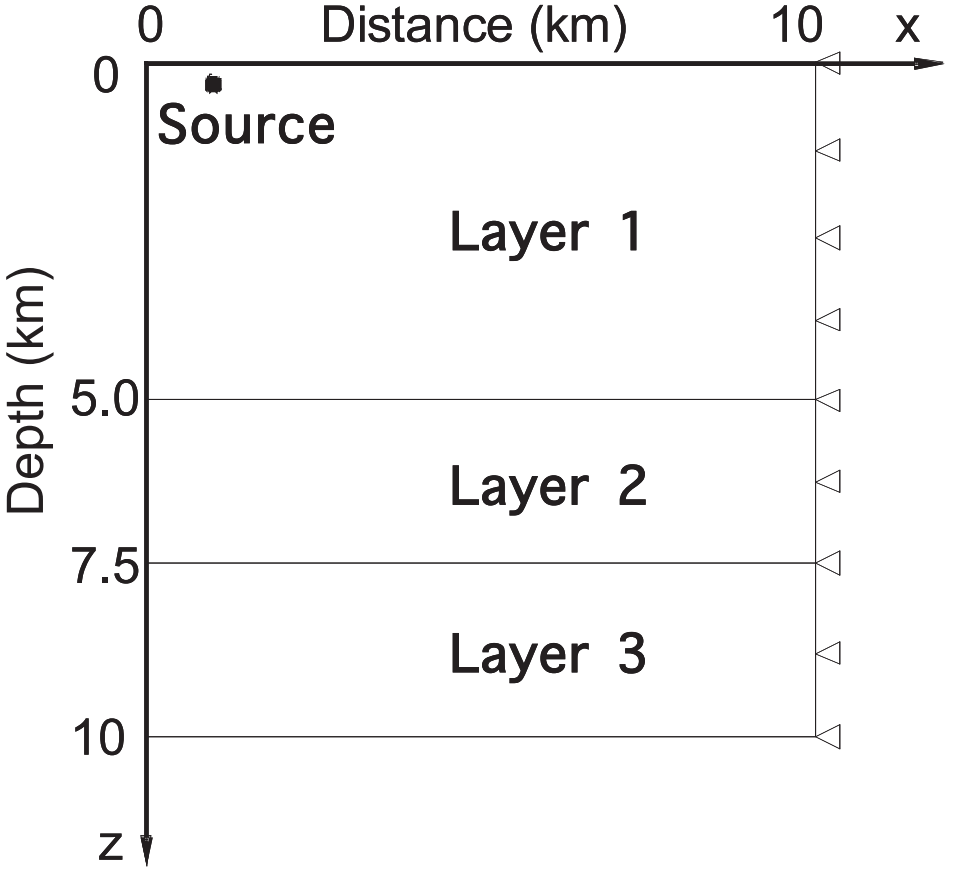

Fig. 10. Three-layer medium model. The explosive source is located at (x_s,z_s) = (1.45 km, 0.3 km). Mechanical properties of the three-layer anisotropic medium model are listed in Table 2.

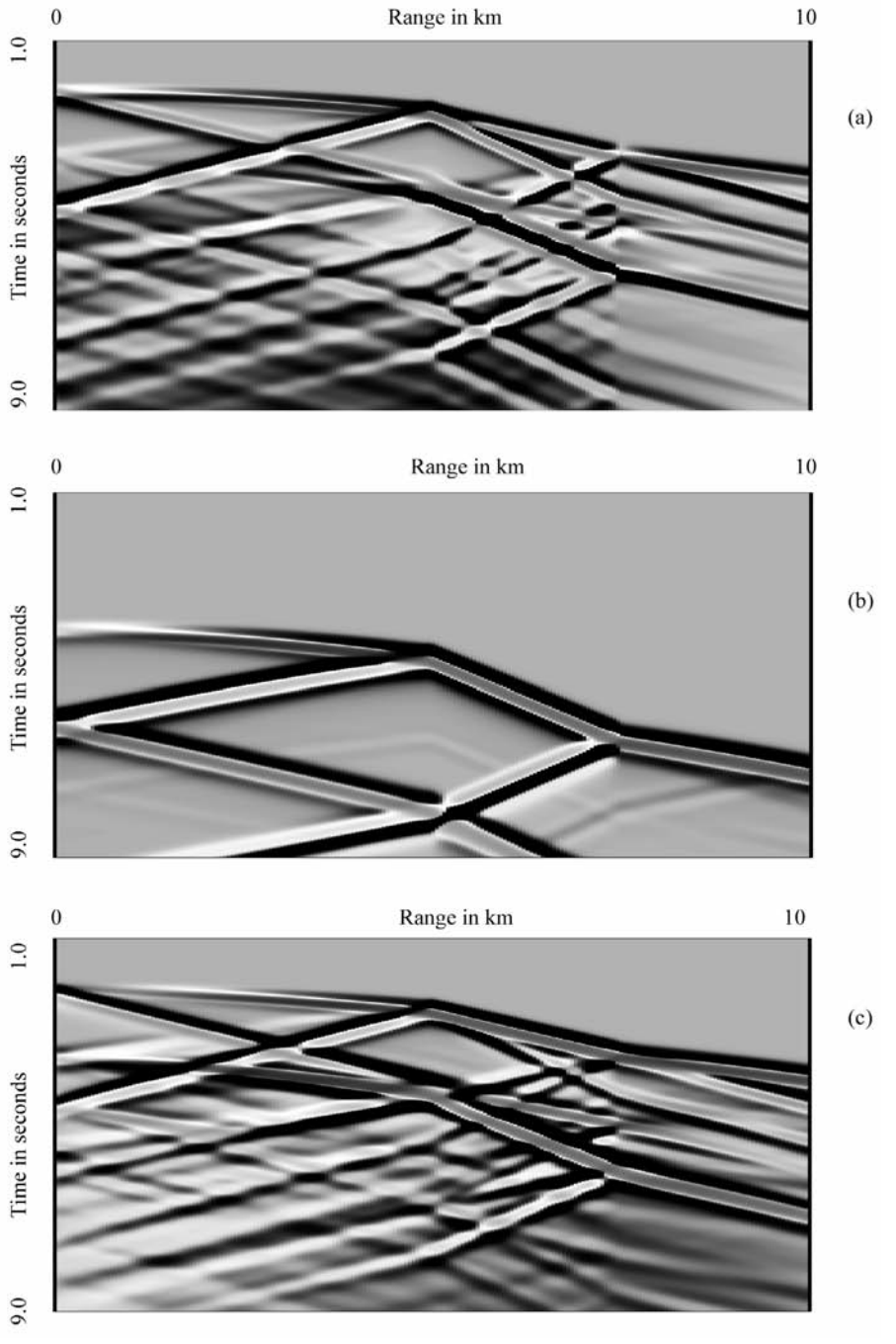

Fig. 11. Three-component synthetic seismograms for the three-layer anisotropic medium model, generated by the modified NADA, for (a) u_x component, (b) u_y component, (c) u_z component. The wavefields are recorded in the well by 201 receivers for the tree-layer anisotropic model shown in Fig. 10 spread from the surface ($z = 0$) to the depth of 10 km spaced 50 m apart.

Synthetic VSP seismograms of three components are shown in Fig. 11. From Fig. 11 we can see that the VSP seismograms are very clean and have no grid dispersions while the model velocity contrasts between adjacent layers (layers 1 and 2, layers 2 and 3) are about 65% for the qP wave and 104% for the qS wave, respectively. In Fig. 11, the qP-, qS-waves, and the reflected, transmitted, and converted waves can be clearly identified. We can also observe the different arrival times of qP- and qS-waves from the synthetic VSP seismograms presented in Fig. 11. Furthermore, we can also see that the numerical computing is still stable at the inner interface of the anisotropic medium with large velocity contrasts between adjacent layers. On the same computer, it took the algorithm about 6 min to generate Fig. 11(b) and 16 min to simultaneously generate Figs. 11(a) and 11(c).

SUMMARY

We have modified the NAD-type methods by replacing particle-velocity $\bar{W}^{n}_{i,j}$ in eq. (2b) with the up-to-date $\bar{W}^{n+1}_{i,j}$ in eq. (3b), which are recently developed by Yang et al. (2003a) for modelling seismic wave propagating in single-phase elastic media (Yang et al., 2003a) and in porous two-phase media with saturated fluids (2007a). Strongly curved qP and qS wavefronts are well reproduced by the modified NADA, including cuspidal triangles. As we have seen in our previous numerical examples, the modified algorithm (3) can further minimize the numerical dispersion of the NAD-type methods, whereas its computational costs and storage space are the same as those of the INADM, and it, compared with the original NADM, saves the storage about 37% and increases slightly in the computational costs (Yang et al., 2007a). Numerical computational results show that the modified algorithm can further suppress the numerical dispersion and the source-noise as we take the minimum number (G=2, Dablain, 1986) of grid points per wavelength for eliminating the spatial numerical dispersion. And the computational speed of the modified NADA is roughly 13 times of the fourth-order LWC method and the modified algorithm requires only roughly 45% of storage space of the fourth-order LWC method on a fine grid to achieve the same accuracy as that of the LWC method. This indicates that the modified NADA enables simulating wave propagation in large-scale models and minimize both the computational CPU time and the storage space using the significant maximum spatial increment ($\Delta x_{max} = v_{min}/2f_N$). Our present algorithm also produces very clear wavefield snapshots and synthetic seismograms for anisotropic media even for the large velocity contrasts between adjacent layers and strong anisotropy.

ACKNOWLEDGMENTS

We thank the anonymous reviewer for improving substantially the presentation of the paper. This work was supported by the National Science Fund for Distinguished Young Scholars of China (Grant No. 40725012) and the National Natural Sciences Foundation of China (Grant 40574014).

REFERENCES

Alford, R.M., Kelly, K.R. and Boore, D.M., 1974. Accuracy of finite-difference modeling of the acoustic wave equation. Geophysics, 39: 834-842.

Blanch, J.O. and Robertsson, J.O.A., 1997. A modified Lax-Wendroff correction for wave propagation in media described by Zener elements. Geophys. J. Int., 131: 381-386.

Dablain, M.A., 1986. The application of high-order differencing to the scalar wave equation. Geophysics, 51: 54-66.

Faria, E.L. and Stoffa, P.L., 1994. Finite-difference modelling in transversely isotropic media. Geophysics 59: 282-289.

Fei, T. and Larner, K., 1995. Elimination of numerical dispersion in finite-difference modeling and migration by flux-corrected transport. Geophysics, 60: 1830-1842.

Fornberg, B., 1990. High-order finite differences and pseudo-spectral method on staggered grids. SIAM J. Numeric. Analys., 27: 904-918.

Holberg, O., 1987. Computational aspects of the choice of operator and sampling interval for numerical differentiation in large-scale simulation of wave phenomena. Geophys. Prosp., 35: 629-655.

Huang, B.S., 1992. A program for two-dimensional seismic wave propagation by the pseudospectrum method. Comput. Geosci., 18: 289-307.

Igel, H., Mora, P. and Riollet, B., 1995. Anisotropic wave propagation through finite-difference grids. Geophysics, 60: 1203-1216.

Kelly, K., Ward, R., Treitel, S. and Alford, R., 1976. Synthetic seismograms: a finite-difference approach. Geophysics, 41: 2-27.

Komatitsch, D., Barnes, C. and Tromp, J., 2000. Wave propagation near a fluid-solid interface: A spectral-element approach. Geophysics, 65: 623-631.

Kosloff, D. and Baysal, E., 1982. Forward modeling by a Fourier method. Geophysics, 47: 1402-1412.

Kosloff, D., Reshef, M. and Loewenthal, D., 1984. Elastic wave calculations by the Fourier method. Bull. Seismol. Soc. Am., 74: 875-891.

Mizutani, H., Geller, R.J. and Takeuchi, N., 2000. Comparison of accuracy and efficiency of time-domain schemes for calculating synthetic seismograms. Phys. Earth Planet. Inter., 119: 75-97.

Sei, A. and Symes, W., 1994. Dispersion analysis of numerical wave propagation and its computational consequences. J. Scient. Comput., 10: 1-27.

Vichnevetsky, R., 1979. Stability charts in the numerical approximation of partial differential equations: a review. Math. Comput. Simul., 21: 170-177.

Virieux, J., 1986. P-SV wave propagation in heterogeneous media: Velocity-stress finite-difference method. Geophysics, 51: 889-901.

Wang, S.Q., Yang, D.H. and Yang, K.D., 2002. Compact finite difference scheme for elastic equations. J. Tsinghua Univ. (Sci. & Tech.), 42: 1128-1131 (in Chinese).

Yang, D.H., Liu, E., Zhang, Z.J. and Teng, J., 2002a. Finite-difference modelling in two-dimensional anisotropic media using a flux-corrected transport technique. Geophys. J. Internat., 148: 320-328.

Yang, D.H., Teng, J.W., Zhang, Z.J. and Liu, E., 2003a. A nearly-analytic discrete method for acoustic and elastic wave equations in anisotropic media. Bull. Seismol. Soc. Am., 93: 882-890.

Yang, D.H., Wang, S.Q., Zhang, Z.J. and Teng, J.W., 2003b. n-times absorbing boundary conditions for compact finite difference modeling of acoustic and elastic wave propagation in the 2-D TI Medium. Bull. Seismol. Soc. Am., 93: 2389-2401.

Yang, D.H., Peng, J.M., Lu, M. and Terlaky, T., 2006. Optimal nearly analytic discrete approximation to the scalar wave equation. Bull. Seismol. Soc. Am., 96: 1114-1130.

Yang, D.H., Song, G.J., Chen, S. and. Hou, B.Y., 2007a. An improved nearly analytical discrete method: An efficient tool to simulate the seismic response of 2-D porous structures. J. Geophys. Engin., 4: 70-82.

Yang, D.H., Chen, S. and Li, J.Z., 2007b. A Runge-Kutta method using high-order interpolation approximation for solving 2D acoustic and elastic wave equations. J. Seismic Explor., 16: 331-353.

Yang, K.D., Yang, D.H. and Wang, S.Q., 2002b. Numerical simulation by the staggered grid method for the high frequency limited BISQ equation. Oil Geophys. Prosp., 37: 463-468 (in Chinese).

Zhang, Z.J., Wang, G.J. and Harris, J.M., 1999. Multi-component wavefield simulation in viscous extensively dilatancy anisotropic media. Phys. Earth Planet. Inter., 114: 25-38.

Zheng, H.S. and Zhang, Z.J., 2005. Synthetic seismograms of nonlinear seismic waves in anisotropic media. Chinese J. Geophys., 48: 660-671 (in Chinese).

Zheng, H.S., Zhang, Z.J. and Liu, E.R., 2006. Non-linear seismic wave propagation in anisotropic media using the flux-corrected transport technique. Geophys. J. Int., 165: 943-956.

APPENDIX

EVALUATION OF THE HIGHER-ORDER DERIVATIVES

To approximate the higher-order derivatives included in eqs. (3a) and (3b) using the displacement or the particle-velocity and their gradients, following Yang et al. (2003a, 2007b), we introduce the interpolation function of the spatial steps Δx and Δz as follows

$$G(\Delta x,\Delta z) = \sum_{r=0}^{5} (1/r!)[\Delta x(\partial/\partial x) + \Delta z(\partial/\partial z)]^r V \quad , \tag{A-1}$$

and construct the connection relations between the point (i, j) and its neighboring nodes. For example, at the grid point (i+1, j) we have the following connection relation,

$$\begin{aligned} [G(\Delta x,0)]^n_{i,j} &= V^n_{i+1,j} \quad , \\ [(\partial/\partial\Delta x)G(\Delta x,0)]^n_{i,j} &= \left((\partial/\partial x)V\right)^n_{i+1,j} \quad , \\ [(\partial/\partial\Delta z)G(\Delta x,0)]^n_{i,j} &= \left((\partial/\partial z)V\right)^n_{i+1,j} \quad , \end{aligned} \tag{A-2}$$

and similarly the rest twenty-one connection relations at other seven neighboring nodes can be easily written. Notice that the vector V is defined by $V = (U,W)^T$, where U is the displacement and W is defined by $W = \partial U/\partial t$.

From the twenty-four connection relations at the nodes (i+1,j), (i−1,j), (i,j−1), (i,j+1), (i−1,j−1), (i−1,j+1), (i+1,j−1), and (i+1,j+1), we can obtain the computational equations to approximate the higher-order derivative $(\partial^{m+k}V/\partial x^m\partial z^k)_{i,j}$ $(2 \le m+k \le 5)$ at the grid point (i,j), which are similar to those suggested by Yang et al. (2003a, 2007b). For convenience, we present these approximate equations as follows

$$\partial_{2x}V^n_{i,j} = (2/\Delta x^2)\delta_x^2V^n_{i,j} - (1/2\Delta x)(E_x^1 - E_x^{-1})\partial_xV^n_{i,j} \quad , \tag{A-3}$$

$$\partial_{2z}V^n_{i,j} = (2/\Delta z^2)\delta_z^2V^n_{i,j} - (1/2\Delta z)(E_z^1 - E_z^{-1})\partial_zV^n_{i,j} \quad , \tag{A-4}$$

$$\begin{aligned}\partial_{3x}V^n_{i,j} = {} & (15/2\Delta x^3)(E_x^1 - E_x^{-1})\partial_xV^n_{i,j} \\ & - (3/2\Delta x^2(E_x^1 + 8I + E_x^{-1})\partial_xV^n_{i,j} \quad ,\end{aligned} \tag{A-5}$$

$$\begin{aligned}\partial_{3z}V^n_{i,j} = {} & (15/2\Delta z^3)(E_z^1 - E_z^{-1})\partial_xV^n_{i,j} \\ & - (3/2\Delta z^2)(E_z^1 + 8I + E_z^{-1})\partial_zV^n_{i,j} \quad ,\end{aligned} \tag{A-6}$$

$$\begin{aligned}\partial_{2xz}V^n_{i,j} = {} & (1/4\Delta x^2\Delta z)(5E_x^1E_z^1 - 5E_x^{-1}E_z^{-1} + E_x^1E_z^{-1} - E_x^{-1}E_z^1 \\ & - 4E_z^1 + 4E_z^{-1} - 6E_x^1 + 6E_x^{-1})V^n_{i,j} \\ & + (1/2\Delta x\Delta z)(-E_x^1E_z^1 - E_x^{-1}E_z^{-1} + E_x^1 + E_x^{-1} - 2\delta_z^2)\partial_xV^n_{i,j} \\ & + (1/\Delta x^2)\delta_x^2(\partial_zV^n_{i,j}) \quad ,\end{aligned} \tag{A-7}$$

$$\begin{aligned}\partial_{x2z}V^n_{i,j} = {} & (1/4\Delta x\Delta z^2)(5E_x^1E_z^1 - 5E_x^{-1}E_z^{-1} - E_x^1E_z^{-1} + E_x^{-1}E_z^1 \\ & - 4E_x^1 + 4E_x^{-1} - 6E_z^1 + 6E_z^{-1})V^n_{i,j} \\ & + (1/2\Delta x\Delta z)(-E_x^1E_z^1 - E_x^{-1}E_z^{-1} + E_z^1 + E_z^{-1} - 2\delta_x^2)\partial_zV^n_{i,j} \\ & + (1/\Delta z^2)\delta_z^2(\partial_xV^n_{i,j}) \quad ,\end{aligned} \tag{A-8}$$

where $\delta_z^2V^n_{i,j} = V^n_{i,j+1} - 2V^n_{i,j} + V^n_{i,j-1}$, $E_z^1V^n_{i,j} = V^n_{i,j+1}$, $E_z^{-1}V^n_{i,j} = V^n_{i,j-1}$. The operators δ_x^2, E_x^1, and E_x^{-1} can be similarly defined. And, $V^n_{i,j}$, $\partial_xV^n_{i,j}$, $\partial_zV^n_{i,j}$ and $\partial_{mxkz}V^n_{i,j}$,denote V(iΔx,jΔz,nΔt), $(\partial/\partial x)$V(iΔx,jΔz,nΔt), $(\partial/\partial z)$V(iΔx,jΔz,nΔt) and $(\partial^{m+k}V/\partial x^m\partial z^k)^n_{i,j}$, respectively. Following Yang et al. (2003a, 2007b), we can similarly write other approximate equations of the higher-order spatial derivatives of the vector V. These equations are here omitted.